Case Studies in Thermal Engineering 47 (2023) 103064

Contents lists available at ScienceDirect

Case Studies in Thermal Engineering

journal homepage: www.elsevier.com/locate/csite

Thermal transport and characterized flow of trihybridity Tiwari and Das Sisko nanofluid via a stenosis artery: A case study

Fu Fangfang [a], Tanveer Sajid [b], Wasim Jamshed [b,*], Mohamed R. Eid [c,d], Gilder Cieza Altamirano [e,f], Imran Altaf [g], Assmaa Abd-Elmonem [h], Sayed M. El Din [i]

[a] School of Education, Nanchang Institute of Science & Technology, Nanchang, 330108, Jiangxi, China
[b] Department of Mathematics, Capital University of Science and Technology (CUST), Islamabad, 44000, Pakistan
[c] Department of Mathematics, Faculty of Science, New Valley University, Al-Kharga, Al-Wadi Al-Gadid, 72511, Egypt
[d] Department of Mathematics, Faculty of Science, Northern Border University, Arar, 1321, Saudi Arabia
[e] Universidad Nacional Autónoma de Chota, Cajamarca, Perú
[f] Fizmako Research Group, Bogotá, Colombia
[g] Institute of Microbiology, University of Veterinary and Animal Science, Lahore, Pakistan
[h] Department of Mathematics, College of Science, King Khalid University, Abha, Saudi Arabia
[i] Center of Research, Faculty of Engineering, Future University in Egypt, New Cairo, 11835, Egypt

A R T I C L E I N F O

Handling Editor: Dr Y Su

Keywords:
Ternary hybrid nanofluid
Sisko fluid
Viscous dissipation
Keller box method
Joule heating
Tiwari and Das model

A B S T R A C T

The improvement of heat transfer is the focus of this paper's innovative theoretical ternary hybridity nanofluid (HNF) prototype. In this examination, blood is employed as the conventional liquid, and the tri-hybrid nanomolecules Au, Ag, and TiO_2 are submerged in it. The extension has been made in the conventional Tiwari and Das hybrid nanofluid model to transform it for the case of a trihybrid nanofluid. By consuming resemblance variables and the Keller box methodology (KBM) to resolve the ordinary differential equations (ODEs) resulting from the conversion of the liquid flowing and temperature formulas. The results are graphed, and it is shown that the trihybridity nanofluid (THNF) has greater thermal conductance than the HNF. The heat transference rate increases in the situation of an augmentation in thermal conduction and radiation effect which helps remove the toxic plaque from the blood flowing through arteries. This additional heat produced because of amplification in thermal radiative fluxing is used to open rigid arteries through which the blood is flow.

1. Introduction

A particular fluid can flow intimate an escalating or constricting conduit with permeable walls, allowing the liquid to enter or depart, to replicate certain fluid movements in biological organisms [1]. This practical model may be used to study the hybrid nanofluid (HNF) movement performance intimate the lymphatic, effervescent diaphragms, percolation, blood current, synthetic dialysis, dual fume dissemination, blood, and air movement in the breathing system, as healthy as medication administration. Sarwar et al. [2] achieved the computational solutions of plasma flowing via a stenosed vein and furthermore investigated the heat transference rate of plasma flowing via these veins. These are some critically significant situations. As the two primary biological filters in our bodies, the kidneys and respiratory system, outflow from the side end of the passageway bedsteads and equivalent reappearance

* Corresponding author.
E-mail address: wasiktk@hotmail.com (W. Jamshed).

https://doi.org/10.1016/j.csite.2023.103064
Received 20 January 2023; Received in revised form 25 March 2023; Accepted 10 May 2023
Available online 19 May 2023

movement at the intravenous end are critical to the mass transmission of different key components concerning blood and material. Padma and Selvi [3] scrutinized the effect of magnetic field and slip conditions on nanofluid moving through a stenotic artery. This modeling might be a useful and thorough representation since the respiratory system is crucial for the movement of mass, oxygen, and other biological factors [4,5].

Using a novel mass-based model of blood HNF movement in the direction of an impermeable stretched slip, Jalili et al. [6] achieved both numerical and analytic solutions of blood flowing through a slanted vein having moderate stricture and investigated the outcome of hybrid nanofluid on the blood flowing to probe thermal performance. Since pure blood serves as the foundation of our model, it is noted by Ijaz et al. [7]. Electroosmotic forces' effect on blood flow through diseased were interrogated by Sara et al. [8]. Gandhi et al. [9] explored the heat transfer effect of blood flow subjected to the bell-shaped occluded artery with the inclusion of effects like viscous dissipation and Joule heating. The influence of inclined magneto force on the blood flowing across a stenosed vein was deliberated by Sharma et al. [10]. While broad blood arteries exhibit the reverse behavior and act like Newtonian fluids, slender blood containers, where the pressure gradient is greater, are more pronounced in their non-Newtonian nature. The shape under study is a bigger artery, therefore Shahzadi and Bilal [11] presented a reasonable study to anticipate that blood behavior will follow Newtonian laws.

Applications for ternary hybrid nanofluids (THNFs) have newly been proposed in the study of blood flow. Dolui et al. [12] examined the current and rapidity slide possessions on the movement of blood using the THNFs model with the inclusion of a combined magnetic field and thermal-based radiation. Saleem et al. [13] studied the thermal of cilia-motivated transition of diffused blood-based THNFs in the exploit of slanted magneto force. Abeer et al. [14] studied the drug delivery aspect of blood-based tri-hybridity fluid flowing via a punctured vessel and detected that the heat transference rate amplifies because of enlargement in the thermal radiative effect. Sajid et al. [15] implemented a newly developed tetra hybrid nanoliquid prototype on the blood flowing through a stenotic artery concerning thermal radiation and Cross non-Newtonianism liquid type. Riaz et al. [16] considered the understanding of the cilia signal of electrically directing Cu-blood THNFs through an unchanging curled frequency when entropy generation is substantial. Rathore and Sandeep [17] designed a computational framework for the invention of a hybrid nanofluid with respect to blood as a conventional liquid flow through the stenotic artery. Abidi et al. [18] presented review studies on the advantages of THNFs including the blood-base flow. Gandhi et al. [19] investigated EMHD impact on the blood flowing via the stenosed vein.

A fundamental model for representing movement in the Newtonian and power-law dominions is the Sisko fluid model (SFM) [20]. Recently, the SFM are applied to simulate the performance of blood flow. Sarwar and Hussain [21] analyzed the influence of gold nanomolecules on the blood flowing via the stenotic vein. Almaneea [22] interrogated the heat transfer aspect of SFM with the utilization of thermal radiation and hybrid nanoparticles in blood and came up with a decision that the incorporation of nanoparticles in the blood increases heat transfer of the blood. Numerical studies are presented in the case of blood flowing via vessel with the consideration of the heat flux model by Foong et al. [23] and Waqas et al. [24]. Bilal and Saeed [25] achieved the numerical solution of SFM flow subjected to contracting/expanding disk accompanied with nanoparticles.

Additionally, due to their extensive use in physiological therapies, magnetohydrodynamics (MHD) and heat transfer have attracted an excessive amount of attention. Recent noteworthy MHD investigations are reported by many authors. Elelamy et al. [26] explored the blood movement of MHD non-Newtonian THNFs with temperature assignment and slide properties, where the implementation of microbial evolution in the heart regulator is suggested. Dahab et al. [27] consumed the frequency movement of MHD Sisko liquid owing to the peristalsis with the addition of consequences such as heat generating (absorbing) and Joules heating. Kumar et al. [28] presented a presentation of thermal source and biochemical response in MHD blood movement via permeable split channels with motivated magnetic field in tumor actions. Dadhich et al. [29] inspected the effect of viscid dissipative flowing and mixed convection on magneto Sisko fluid flow subjected to a wedge. Another fractional model is presented by Majeed et al. [30]. Tanveer et al. [31] deduced the theoretical examination of peristaltic movement in magneto blood flow of non-Newtonianism substances. Yin et al. [32] studied the behavior of microbes and nanomolecules on Sisko fluid flowing via a stretching tube. Ahmed et al. [33] investigated the covalent bonding relationship between molecules of Sisko fluid flow towards a curved surface accompanied by a magnetic field effect. Kumawat et al. [34] computed the irreversibility phenomenon of magnetized blood flowing via a penetrable artery underneath the effect of varying viscosity.

Due to possible applications in public health, a study on the effects of heat radiation and double diffusion is crucial. Additionally, because blood includes ions that make up an electric current, the hall-effect may be utilized to gauge blood movement frequency. Sreedevi et al. [35] examined heat and mass transfer analysis of nanofluid accompanied by effects like thermal-based radiation and chemical reaction flow over expendable sheets having linear as well as nonlinear in nature. Asha et al. [36] explored the behavior of gold nanomolecules on the peristaltic movement of blood with the inclusion of thermal radiation in the instance of Jeffrey liquid with a double diffusion effect. Abd-Alla et al. [37] contemplated the peristaltic phenomenon of blood flow through a symmetric channel under the influence of inclined magneto force. Kumar et al. [38] probed the impact of heat sources and chemical reactions on magnetized blood flow through permeable arteries for tumor treatment. The impact of ternary nanomolecules and magneto force on cilia-actuated transport of blood flow was explored deeply by Saleem et al. [39]. Manjunatha et al. [40] probed the influence of ternary hybrid nanoparticles on blood flow over a bi-directional slippery surface and remarked that heat transference rate magnifies extra in the presence of ternary nanomolecules. biomedical features of entropy generating on MHD blood movement of THNFs with non-linearly current energy and non-uniformly temperature generating (sinking).

In many systems that are susceptible to significant fluctuations in gravitational force or that operate at high speeds, the viscous dissipation and Joule heating (VD&JH) effect is a key factor in natural convection. Gandhi et al. [41] modeled and analyzed MHD of HNF-gold blood-based preparation distribution through a bell-shaped obstructed artery with VD&JH and variable viscosity possessions. The effect of a magnetic field on stagnated hybrid nanofluid accompanied by viscous dissipation and Joules heating was interrogated in detail by Zainal et al. [42]. Venkatesan and Reddy [43] introduced a vision into the changing aspects of blood assigning alumina HNF related to Lorentz force, VD&JH, thermal radiative, and heat generating. Waini et al. [44] investigated the performance of $CoFe_2O_4$–TiO_2 hybridity nanomolecules on micropolarity liquid flowing subjected to an expandable medium accompanied with VD effect. Sridhar et al. [45] evaluated the thermal radiative fluxing and VD&JH possessions on blood-Au couple stress HNF flowing determined by electroosmosis. Sulochana and Shivapuji [46] numerically achieved the solution of hybrid nanofluid accompanied with VD & JH effects.

One of the numerical approaches for tackling issues is KBM, which is an implied procedure for lessening a collection of ODEs to a scheme of 1st-order DEs. Many scholars that study THNFs and HNFs, in general, utilize the KBM extensively. To increase the thermal efficacy, proportional analysis, mono phase analysis, thermal expansion optimisation, and computational efforts with the utilization of KBM and various types of THNFs. Anwar et al. [47] utilized the Keller box scheme to achieve the numerical solution of magneto Williamson nanoliquid flowing towards an inclined sheet. Arif et al. [48] achieved the solution of 2nd-grade liquid accompanied by hybridity nanomolecules and activation energy sense with the help of KBM. Shi et al. [49] scrutinized the behavior of micropolar liquid past an exponentially curved surface and furthermore solved the proposed model numerically with the utilization of KBM. Jamshed et al. [50] investigated the consequences of magnetic nanoparticles on Eyring Powell liquid and handled the model numerically with the help of the KBM scheme. Ahmed et al. [51] scrutinized diffusion thermo/thermo diffusion effect on third-grade liquid flow across an expanding cylinder and solved the modeled PDEs numerically with the utilization of KBM. Alwawi et al. [52] optimized the HT by MHD THNFs across a cylinder using the KBM. Ullah et al. [53] explored the heat and mass transference analysis of Casson nanofluid past a porousness wedge accompanied by MHD and chemical reaction effect and achieved the solution with the KBM technique. Numerical solutions with the help of KBM for the situation of micropolar liquid flowing via a curved surface with the help of KBM were presented by Shabbir et al. [54]. Numerical investigations based on KBM were given by Kumaran et al. [55].

1.1. Motivation

Nanoparticles are effective in the treatment of cardiovascular diseases. The attributes and physical properties of nanomolecules like size, structure, and surface provide improved treatment plans in terms of cures for cardiovascular diseases, and the transport of nanomolecules into the arteries mostly relies on their physical properties of nanoparticles. Research throughout the world has endeavoured to find the effect of nanoparticles on the blood flowing through blood vessels with the insertion of diverse impacts. The motive behind this examination is to discover the impact of trihybrid nanomolecules on the blood flowing via veins in the presence of magnetism force, thermal-based conduction, and thermal radiation. Tiwari and Das hybrid nanoparticles have been expanded for the status of tri-hybridity nanomolecules. This work becomes novel after the inclusion of the trihybrid Tiwari and Das model with the inclusion of MHD, Joule's heating, dissipation effect, and thermal radiation. Additional heat is produced in the status of trihybridity nanomolecules which are used for various purposes like the elimination of toxic materials from the blood and opening of rigid arteries.

1.2. Novelty

The novelty behind the present research is given below.

- Extension has been made in one-phase hybridity nanoliquid prototype to transform it into a ternary hybrid nanofluid.
- Heat transference examination in the status of trihybridity nanomolecules passed a stenosed with the consideration of magnetism force consequence is never studied yet in the available literature with the consideration of combined thermal radiative, viscidness dissipative, Cattaneo-Christov heat flux and Joule's heat up effect.

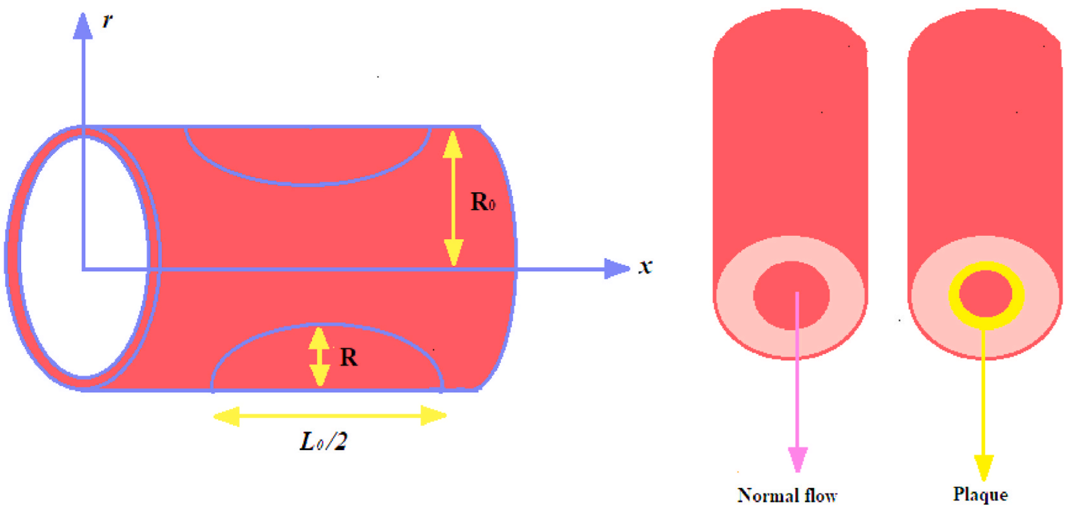

Fig. 1. Visual illustration of typical blood flowing via vessel with plaque.

2. Mathematical formulation

Fig. 1 is constructed to reveal the behaviour of blood-flowing veins having a length $\frac{L_0}{2}$ with regard to the Sisko liquid type. Magneto force is utilized in the path normal to the blood flowing. The temperature effect of the fluid is inspected with the inclusion of diverse phenomena such as the Cattaneo-Christov heating flux model is also considered to inspect the outcome of heat transference for the case of blood flow stenotic arteries, Joule heating, viscid-dependent dissipative flow as well as thermal-based radiations. The extended Tiwari and Das nanofluid paradigm has been considered to study the influence of three diverse types of nanomolecules on the blood flow through veins. Blood is running alongside $x-$ path and $r-$ path deemed perpendicular to the blood flow and blood flow through arteries forms a consent-type shape curve. The symbols $R(x)$ and λ indicate the radius for the case of the artery and the maximum height in the case of stenosis.

Mathematical expression of the stenosed region is given by

$$R(x) = R_0 - \frac{\lambda}{2}\left(1 + cos\left(\frac{4\pi x}{L_0}\right)\right), \frac{-L_0}{4} < x < \frac{L_0}{4} = R_0 \text{ Otherwise}$$

The modeled Eqs. (1)–(3) are derived from impetus preservation law, the Navier-Stokes equation, and the second law of thermodynamics beneath the effect of boundary layer assumptions. The governing modeled PDEs are given by

$$\frac{\partial(ru)}{\partial x} + \frac{\partial(rv)}{\partial r} = 0, \tag{1}$$

$$\rho_{thnf}\left(u\frac{\partial u}{\partial x} + v\frac{\partial u}{\partial r}\right) = \frac{\mu_{thnf}}{r}\frac{\partial}{\partial r}\left(r\frac{\partial u}{\partial r}\right) - \frac{\alpha}{r}\frac{\partial}{\partial r}\left(r\left(-\frac{\partial u}{\partial r}\right)^n\right) - \sigma_{thnf}B_0{}^2u, \tag{2}$$

$$\begin{aligned}(\rho C_p)_{thnf}\left(u\frac{\partial T}{\partial x} + v\frac{\partial T}{\partial r}\right) + \beta_1\left(u^2\frac{\partial^2 T}{\partial x^2} + 2uv\frac{\partial^2 T}{\partial x\partial r} + v^2\frac{\partial^2 T}{\partial r^2} + \frac{\partial T}{\partial x}\left(u\frac{\partial T}{\partial x} + v\frac{\partial T}{\partial r}\right) + \frac{\partial T}{\partial r}\left(u\frac{\partial T}{\partial x} + v\frac{\partial T}{\partial r}\right)\right) = \frac{k_{thnf}}{r}\frac{\partial}{\partial r}\left(r\frac{\partial T}{\partial r}\right) + \frac{\partial}{\partial r}\left(\frac{16\sigma^* T_\infty^3}{3\kappa^*}\frac{\partial T}{\partial r}\right) \\ + \mu_{thnf}\left(-\frac{\partial u}{\partial r}\right)^2 + \alpha\left(-\frac{\partial u}{\partial r}\right)^{n+1} + \sigma_{thnf}B_0{}^2u^2.\end{aligned} \tag{3}$$

The accompanying boundary constraints are:

$$\left.\begin{array}{l} r = R : u = u_0, v = 0, T = T_w, \\ r \to \infty : u \to 0, T \to T_\infty. \end{array}\right\} \tag{4}$$

Descriptions regarding the thermophysical attributes for ternary hybridized nanoliquid offered by

$$\left.\begin{array}{l} \mu_{thnf} = \dfrac{\mu_f}{(1-\varphi_1)^{2.5}(1-\varphi_2)^{2.5}(1-\varphi_3)^{2.5}}, \\ \rho_{thnf} = \left[(1-\varphi_1)\left\{(1-\varphi_2)\left[(1-\varphi_3)\rho_f + \rho_3\varphi_3\right] + \rho_2\varphi_2\right\} + \rho_1\varphi_1\right], \\ (\rho C_p)_{thnf} = (1-\varphi_1)\left\{(1-\varphi_2)\left[(1-\varphi_3)(\rho C_p)_f + (\rho C_p)_{s_3}\varphi_3\right] + ,\right. \\ \left.(\rho C_p)_{s_2}\varphi_2\right\} + (\rho C_p)_{s_1}\varphi_1 \end{array}\right\} \tag{5}$$

Thermal conductivity is given by

$$\left.\begin{array}{l} \dfrac{k_{thnf}}{k_{hnf}} = \dfrac{(n-1)k_{hnf} - (k_{hnf} - k_3)\varphi_3(n-1) + k_3}{(k_{hnf} - k_3)\varphi_3 + (n-1)k_{hnf} + k_3}, \\ \dfrac{k_{hnf}}{k_{nf}} = \dfrac{(n-1)k_{nf} - (k_{nf} - k_2)\varphi_2(n-1) + k_2}{(k_{nf} - k_2)\varphi_2 + (n-1)k_{nf} + k_2}, \\ \dfrac{k_{nf}}{k_f} = \dfrac{(n-1)k_f - (k_f - k_1)\varphi_1(n-1) + k_1}{(k_{nf} - k_1)\varphi_1 + (n-1)k_f + k_2} \end{array}\right\} \tag{6}$$

Electrical conductivity is given by

Table 1
Thermo-physical attributes.

Attributes	Blood	Au	TiO_2	Ag
ρ	1050	19300	4250	10500
C_p	3617	129	690	235
k	0.52	310	8.953	429
σ	0.667	4.1×10^6	2.4×10^6	6.3×10^7

$$\left.\begin{aligned}\frac{\sigma_{thnf}}{\sigma_{hnf}}&=\frac{(1+2\varphi_3)\sigma_3+(1-2\varphi_3)\sigma_{hnf}}{(1-\varphi_3)\sigma_3+(1+\varphi_3)\sigma_{hnf}},\\ \frac{\sigma_{hnf}}{\sigma_{nf}}&=\frac{(1+2\varphi_2)\sigma_2+(1-2\varphi_2)\sigma_{nf}}{(1-\varphi_2)\sigma_3+(1+\varphi_2)\sigma_{nf}},\\ \frac{\sigma_{nf}}{\sigma_f}&=\frac{(1+2\varphi_1)\sigma_1+(1-2\varphi_1)\sigma_f}{(1-\varphi_1)\sigma_1+(1+\varphi_1)\sigma_f},\end{aligned}\right\} \tag{7}$$

Thermophysical properties of TiO_2, Al_2O_3, and SiO_2 nanomolecules and blood as a conventional liquid are described in Table 1. The statement involving Rosseland's guesstimate is

$$q_r=-\frac{4\sigma^*}{3\kappa^*}\frac{\partial T^4}{\partial y}, \tag{8}$$

however σ^* and κ^* comparatively illustrates Boltzmann's fixed value and absorbing factor, correspondingly.

3. Solving methodology

Consider the suitable conversions mentioned above

$$\left.\begin{aligned}&u=\frac{u_0x}{L_0}f^{'}(\eta), v=-\frac{R}{r}\sqrt{\frac{u_0v}{L_0}}f(\eta), \theta(\eta)=\frac{T-T_\infty}{T_w-T_\infty},\\ &\eta=\frac{r^2-R^2}{2R}\sqrt{\frac{u_0}{vL_0}}.\end{aligned}\right\} \tag{9}$$

Eqs. (2)–(4) are translated into the subsequent dimensionless formulas as a consequence of the preceding conversion.

$$(1+2\gamma\eta)f^{'''}+2\gamma f^{'}+A_1S(1+2\gamma\eta)^{\frac{n-1}{2}}(n(1+2\gamma\eta))(-f'')^{n-1}f^{'''}-\gamma(-f'')^n-A_1A_2\left(f^{'2}-f''f\right)-A_1A_2A_3Mf^{'}=0, \tag{10}$$

$$A_5((1+Rd)(1+2\gamma\eta)\theta''+2\gamma\theta^{'})+A_4Prf\theta^{'}+PrEc\left(\frac{(1+2\gamma\eta)}{A_1}f''^2+S(1+2\gamma\eta)^{\frac{n+1}{2}}(-f'')^n\right)+A_3MPrEcf^{'2}-A_4\,Pr\,\lambda_1\left(f^2\theta''+ff^{'}\theta^{'}\right)=0, \tag{11}$$

The boundary constraints (5) change to the subsequent structure:

$$\left.\begin{aligned}&\eta=0:f(\eta)=0,f^{'}(\eta)=1,\theta=1,\\ &\eta\to\infty:f^{'}(\eta)\to 0,\theta(\eta)\to 0.\end{aligned}\right\} \tag{12}$$

The next non - dimensional variables are derived from Eqs. 10–12:

$$\left.\begin{aligned}&S=\frac{\alpha}{\mu_f}\left(\frac{u_0x}{L_0}\sqrt{\frac{u_0}{v_fL_0}}\right)^{n-1}, \gamma=\sqrt{\frac{v_fL_0}{u_0R^2}}, Ec=\frac{u_0^2x^2}{C_{p_f}(T_w-T_\infty){L_0}^2},\\ &Rd=\frac{16\sigma T_\infty^3}{3k^*k_\infty}, Pr=\frac{(\mu C_p)_f}{k_f}, M=\frac{L_0\sigma_fB_0^2}{\rho_fu_0}, \lambda_1=\frac{\beta_1u_0}{L_0}.\end{aligned}\right\}$$

The Nusselt amount and local wall friction component are supplied by

$$Cf=\frac{2\tau_w}{\rho_fu_w^2}, Nu_x=\frac{xq_w}{k_f(T_w-T_\infty)}, \tag{13}$$

whereas the shear stresses τ_{xz}, τ_{yz}, surface heat fluxing q_w are intended by

$$\tau_w=\mu_{thnf}\frac{\partial u}{\partial r}-\alpha\left(-\frac{\partial u}{\partial r}\right)^n, q_w=-k_{thnf}\frac{\partial T}{\partial r}. \tag{14}$$

The non-dimensional way of frictional force is characterized by

$$CfRe_x^{1/2}=\frac{1}{A_1}f''-S(-f'')^n, \tag{15}$$

It is conferred by the non-dimensional Nusselt number

$$Nu_xRe_x^{-1/2}=-A_5\theta^{'} \tag{16}$$

whereas A_1, A_2, A_3, A_4 and A_5 are given by

$$\left.\begin{aligned}
A_1 &= \frac{1}{(1-\varphi_1)^{2.5}(1-\varphi_2)^{2.5}(1-\varphi_3)^{2.5}},\\
A_2 &= (1-\varphi_1)\left\{(1-\varphi_2)\left[(1-\varphi_3)+\varphi_3\frac{\rho_3}{\rho_f}\right]+\varphi_2\frac{\rho_2}{\rho_f}\right\}+\varphi_1\frac{\rho_1}{\rho_f},\\
A_2 &= \frac{\sigma_{thnf}}{\sigma_f},\\
A_4 &= (1-\varphi_1)\left\{(1-\varphi_2)\left[(1-\varphi_3)+\frac{(\rho C_p)_{s_3}}{(\rho C_p)_f}\varphi_3\right\}+\frac{(\rho C_p)_{s_2}}{(\rho C_p)_f}\varphi_2\right\}+\frac{(\rho C_p)_{s_1}}{(\rho C_p)_f}\varphi_1,\\
A_5 &= \frac{k_{thnf}}{k_f}.
\end{aligned}\right\} \tag{17}$$

4. Keller box method: 2nd order convergent

4.1. Methodology

The Keller-box procedure is managed to solve Eqs. (9) and (11) subject to boundary constraints (12). Despite recent developments in other numerical approaches, this process appears to be the least adaptable of the basic ways, and it continues to be a strong and very reliable solution for parabola boundary layer fluxes. It can also solve problems of any order and is unconditionally stable on outcomes. A flow process chart (Fig. 1S) depicts KBM stage-by-stage approach.

4.2. Transformation of ODEs

We begin with establishing new independent variables: $\Omega y_1(x,\eta)$, $\Omega y_2(x,\eta)$, $\Omega y_3(x,\eta)$, $\Omega y_4(x,\eta)$ and $\Omega y_5(x,\eta)$ with $\Omega y_1 = f, \Omega y_2 = f^{'}, \Omega y_3 = f'', \Omega y_4 = \theta$ and $\Omega y_5 = \theta^{'}$. Given these conversions, Eqs. 9–12 is diminished to the subsequent 1st-order structure

$$\frac{d\Omega y_1}{d\eta} = \Omega y_2, \tag{18}$$

$$\frac{d\Omega y_2}{d\eta} = \Omega y_3, \tag{19}$$

$$\frac{d\Omega y_4}{d\eta} = \Omega y_5, \tag{20}$$

$$(1+2\gamma\eta)\Omega y_3{}' + 2\gamma\Omega y_2 + A_1 S(1+2\gamma\eta)^{\frac{n-1}{2}}(n(1+2\gamma\eta))(-\Omega y_3)^{n-1}\Omega y_3{}' - \gamma(-\Omega y_3)^n - A_1A_2\left(\Omega y_2{}^2 - \Omega y_3\Omega y_1\right) - A_1A_2A_3M\Omega y_2 = 0, \tag{21}$$

$$A_5((1+Rd)(1+2\gamma\eta)\Omega y_5{}' + 2\gamma\Omega y_5) + +A_3MPrEc\Omega y_2^2 + A_4\,Pr\,\Omega y_1\Omega y_5 + PrEc\left(\frac{(1+2\gamma\eta)}{A_1}\Omega y_3{}^2 + S(1+2\gamma\eta)^{\frac{n+1}{2}}(-\Omega y_3)^n\right) - A_4\,Pr\,\lambda_1\left(y_1^2 y_5^{'}\right.$$
$$\left. + y_1y_3y_5\right) = 0, \tag{22}$$

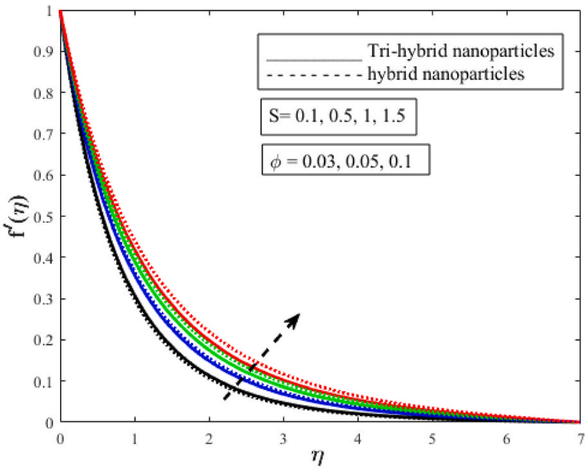

Fig. 2. Consequences of S values change on $f^{'}(\eta)$.

$$\left.\begin{array}{l}\eta=0:\Omega y_1(0)=0,\Omega y_2(0)=1,\Omega y_4(0)=1,\\ \eta\to\infty:\Omega y_2\to 0,\Omega y_4\to 0.\end{array}\right\} \tag{23}$$

4.3. Difference equations and domains discretizing

In addition, domain discretizing in the $x-$ axis is depicted in Fig. 2S. Net points are defined in light of this mesh $\eta_0=0,\eta_j=\eta_{j-1}+\delta h, j=0,1,2,3...,J,\eta_J=1$ where δh is the step size.

Applying central differences formulation at the midpoint $\eta_{j-1/2}$.

$$2\left((\Omega y_1)_j-\left((\Omega y_1)_{j-1}\right)=\delta h\left((\Omega y_2)_j-(\Omega y_2)_{j-1}\right),\right. \tag{24}$$

$$2\left((\Omega y_2)_j-\left((\Omega y_2)_{j-1}\right)=\delta h\left((\Omega y_3)_j-(\Omega y_3)_{j-1}\right),\right. \tag{25}$$

$$2\left((\Omega y_4)_j-\left((\Omega y_4)_{j-1}\right)=\delta h\left((\Omega y_5)_j-(\Omega y_5)_{j-1}\right),\right. \tag{26}$$

$$\begin{aligned}&(1+2\gamma\eta)\left(\frac{\left((\Omega y_3)_j-\left(\Omega y_3\right)_{j-1}\right)}{\delta h}\right)+2\gamma\left(\frac{(\Omega y_2)_j-(\Omega y_2)_{j-1}}{2}\right)+A_1S\left(-\frac{(\Omega y_3)_j-(\Omega y_3)_{j-1}}{2}\right)^n-A_1A_2\left(\left(\frac{(\Omega y_2)_j-(\Omega y_2)_{j-1}}{2}\right)^2\right.\\&\left.-\left(\frac{(\Omega y_1)_j-(\Omega y_1)_{j-1}}{2}\right)\left(\frac{(\Omega y_3)_j-(\Omega y_3)_{j-1}}{2}\right)\right)-A_1A_2A_3\left(\frac{(\Omega y_2)_j-(\Omega y_2)_{j-1}}{2}\right)=0,\end{aligned} \tag{27}$$

$$A_3\Pr\lambda_1\left(\left(\frac{(\Omega y_1)_j-(\Omega y_1)_{j-1}}{2}\right)^2\frac{\left((\Omega y_5)_j-\left(\Omega y_5\right)_{j-1}\right)}{\delta h}+\left(\frac{(\Omega y_1)_j-(\Omega y_1)_{j-1}}{2}\right)\left(\frac{(\Omega y_2)_j-(\Omega y_2)_{j-1}}{2}\right)\left(\frac{(\Omega y_5)_j-(\Omega y_5)_{j-1}}{2}\right)\right)=0 \tag{28}$$

4.4. Newton method

Eqs. 24–28 are linearised by ways of Newtonian linearization methodology

$$\left.\begin{array}{ll}(\Omega y_1)_j^{n+1}=(\Omega y_1)_j^n+\delta(\Omega y_1)_j^n, & (\Omega y_2)_j^{n+1}=(\Omega y_2)_j^n+\delta(\Omega y_2)_j^n,\\ (\Omega y_3)_j^{n+1}=(\Omega y_3)_j^n+\delta(\Omega y_3)_j^n, & (\Omega y_4)_j^{n+1}=(\Omega y_4)_j^n+\delta(\Omega y_4)_j^n,\\ (\Omega y_5)_j^{n+1}=(\Omega y_5)_j^n+\delta(\Omega y_5)_j^n. & \end{array}\right\} \tag{29}$$

4.5. Block tridiagonal form

Following the linearised scheme has the subsequent block tridiagonal form

$$B\Lambda=\varepsilon, \tag{30}$$

wherein

$$B=\begin{bmatrix}[L_1] & [N_1] & & & & & \\ & [L_2] & [N_2] & & & & \\ & & & \ddots & & & \\ & & & \ddots & & & \\ & & & \ddots & & & \\ & & & & [M_{J-1}] & [L_{J-1}] & [N_{J-1}] \\ & & & & & [M_J] & [L_J]\end{bmatrix},\Lambda=\begin{bmatrix}[\Lambda_1]\\ \vdots\\ \vdots\\ \vdots\\ [\Lambda_{J-1}]\\ [\Lambda_J]\end{bmatrix}\text{ and }\varepsilon=\begin{bmatrix}[\varepsilon_1]\\ \vdots\\ \vdots\\ \vdots\\ [\varepsilon_{J-1}]\\ [\varepsilon_J]\end{bmatrix}.$$

Now by factorizing B as

$$B=LU, \tag{31}$$

wherein

$$L=\begin{bmatrix}[\Psi_1] & & & & \\ & [\Psi_2] & & & \\ & & \ddots & & \\ & & \ddots & [\Psi_{J-1}] & \\ & & & [M_J] & [\Psi_J]\end{bmatrix},U=\begin{bmatrix}[I] & [\alpha_1] & & & \\ & [I] & [\alpha_2] & & \\ & & \ddots & \ddots & \\ & & & [I] & [\alpha_{J-1}] \\ & & & & [I]\end{bmatrix},$$

wherein the overall sizing of the block tridiagonal array B is $J\times J$ with all block sizing of supervectors being 5×5 and $[I]$, $[\Psi_i]$ and $[\alpha_i]$ are order 5 arraies. LU decomposition algorithm is utilized to solve Δ. A mesh sizing of $h=0.01$ is determined to be proper for mathematical assessment, and the findings are achieved with an error tolerance of 10^{-5}.

5. Findings and discussion

Fig. 2 is constructed to analyze the impact of the Sisko fluid material variable S on the rapidity field $f'(\eta)$. It is detected from the figure that magnification in S amplifies the fluid velocity. The parameter decides the relation between inertial forces and viscous forces. The inertial forces dominate over viscous powers by the virtue of amplification in S. Pseudo-plastic behavior is detected in the situation of blood flow through vessels. In contrary to trihybrid nanoparticles, the upward movement of the full far from the vertical surface is more pronounced in the case of dihybrid nanoparticles. The viscosity of blood gradually decreases owing to magnification in S which creates a good effect on the human body and avoids heart attacks and strokes. The influence of magnetic variable M on $f'(\eta)$ is highlighted in Fig. 3. It is stated that an electrical conductive liquid with a magnetic field produces a force termed Lorentz forces which makes resistance to the blood flowing through arteries. It may be because, when body fluid is revealed to a magneto force, the activity of magnetized applies a rotating motion to blood electric molecules and magnetic particles, causing them to rotate due to the impact of the magnetic field. An abatement in fluid velocity is seen because the activity of alignment causes the red cells of blood and magneto molecules to be extra suspended in the plasma (liquid). Additionally, an improvement in the concentration of magneto particles can result in a boost in the inner viscidness of the blood. As a result, $f'(\eta)$ diminishes by incorporation of nanomolecules in the traditional fluid also augments the concentration of the body-liquid which amplifies viscid and diminishes $f'(\eta)$. The change of power law index n on $f'(\eta)$ is highlighted in Fig. 4. The variable n determines how much viscous the fluid is. The viscosity of blood increases in the case of $n > 1$, decreases in the situation of $n < 1$, and is Newtonian in the case of $n = 1$. The viscosity of blood increases by the virtue of amplification in n. More resistance is produced and viscous powers control the inertial powers. The viscosity of blood increases which narrows the size of the blood vessel via which blood is flow creating a chance of heart attack, strokes, and arteriosclerosis. It is remarked that the amplification of fractional size of nanomolecules amplifies the concentricity of particles inside the flood which diminishes the velocity of blood flow through arteries. The relation between curvature parameter γ on $f'(\eta)$ is revealed in Fig. 5. It is quite evident that magnification in γ guides amplification in the rapidity of the blood flowing. It is crystal clear that a decrement in a radius of curvature amplifies the curvature parameter and velocity phenomenon. The connection zone amongst the blood fluid and cylindrical wall is lowered and a lesser amount of frictional force is offered in the case of magnification in γ and the body fluid is shifting more frequently via vessels and chances of heart attack and strokes are getting lower.

Changing of Eckart number Ec on temperature field $\theta(\eta)$ is highlighted in Fig. 6. It is well established that an upswing in Ec escalates the temperature of the blood. It is observed that frictional heating is produced owing to magnification in Ec. Eckart number is actually the ratio between kinetic energy to enthalpy difference between the wall and the base fluid. It is perceived that an increasing shift in Ec transforms kinetic into internal energy in terms of work done by any sort of fluid (blood) against the viscous stresses. The heat inside the blood dominates the viscosity phenomenon. This factor is more dominant in the presence of trihybrid nanoparticles because injected nanoparticles in blood enhance the thermal conductivity of the blood and more heat is produced inside the blood which opens the rigid arteries containing plaque and other waste materials. The arteries become less squeezed under the cause of nanomolecules in the conventional liquid. An impact of curvature parameter γ on $\theta(\eta)$ is portrayed in Fig. 3S. The radius of curvature is opposite to curvature. An increment change in γ lessens the radius of curvature and blood fluid is flowing more smoothly through arteries. The curvature parameter also escalates because of the incorporation of nanomolecules injected into the blood. It is also observed that magnification in γ diminishes the surface link area of particles present in the fluid and amplifies the average kinetic energy of the blood. Nanoparticles can boost biological features that decrease complement system activation, lengthen blood circulation times, and lower toxicity by attaching to plasma proteins like albumin. The influence of magnetic variable M on temperature outline is highlighted in

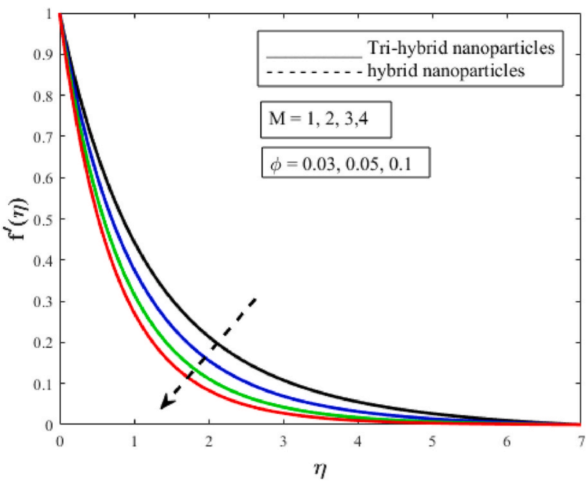

Fig. 3. Consequences of M values change on $f'(\eta)$.

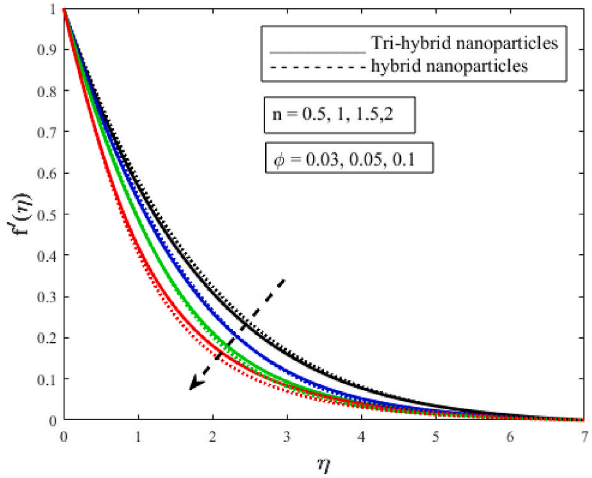

Fig. 4. Consequences of n values change on $f'(\eta)$.

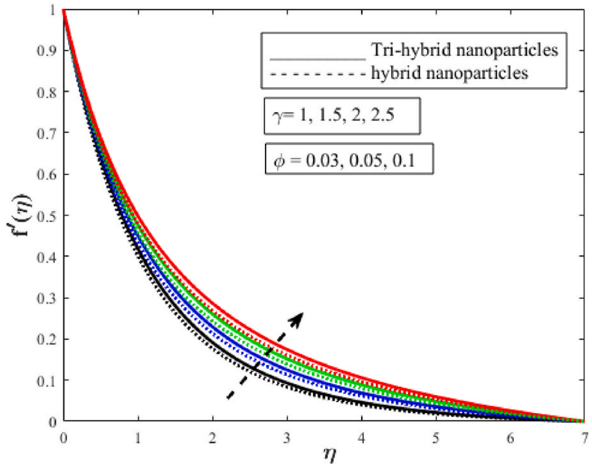

Fig. 5. Effect of γ on $f'(\eta)$.

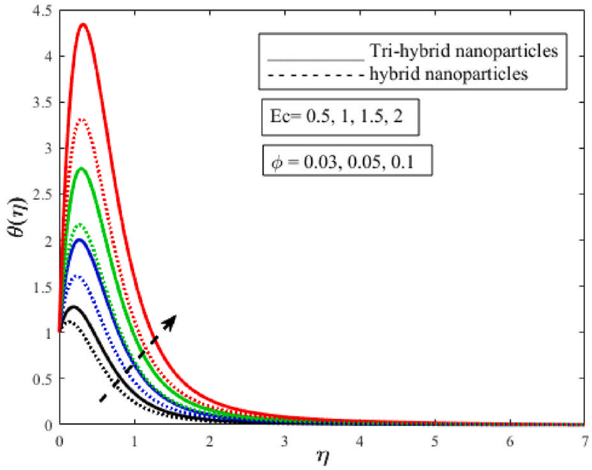

Fig. 6. Consequences of changing Ec values on $\theta(\eta)$.

Fig. 4S. Lorentz force is produced when electrically conducting blood is flowing through arteries which delivers opposition to the blood flowing through arteries. When M gradually changes, the viscosity of blood decreases. Viscosity and temperature are negatively proportionate. The injection of trihybrid nanoparticles like silver, gold, and titanium oxide enhances the temperature of the blood. It is noticed that when viscosity diminishes the temperature within the blood amplifies which amplifies the temperature field. The liquid is going away from the vertical surface and this change is much additional noticeable in the instance of trihybridity nanomolecules in contrast to the dihybridity nanomolecules. An increase in temperature opens the unblocked arteries and removes toxic waste material present in the blood and the blood moves smoothly across the vascular veins. This type of situation helps to avoid strokes and heart attack-type situations. It is remarked that a confident variation in consistency index n amplifies the temperature outline as demonstrated in Fig. 5S. Power law index n is directly linked with viscosity and inversely linked with temperature. Incremental changes in viscosity blocked the arteries but others amplify the temperature with open the squeezed arteries. Both trihybrid nanoparticles and n provide a sufficient temperature that amplifies the temperature inside the blood and it moves effortlessly via the vessels and amplifies the temperature field. Nanoparticles topple the viscosity phenomenon and this alteration is extra prominent in the circumstance of injection of trihybrid nanomolecules instead of dihybrid nanoparticles and eradicates toxic materials present in the blood and is more helpful in the case of a disease like arteriosclerosis in which arteries become rigid and additional temperature is required to open the closed arteries. Prandtl quantity is characterized as an impetus to thermal diffusivity. Heat disperses more swiftly in the situation of enlargement in Pr amounts that depreciate the fluid temperature as shown in Fig. 6S. Heat diffuses more quickly which brings a lacking temperature inside the body fluid and the viscid occurrence dominates which rigid the vessels across the body fluid flow. The blood hardly flows through the squeezing arterial walls. Heat transfer, with temperature within the body fluid, depreciates which diminishes the temperature field. From Fig. 7S it is observed that confident variations in Rd magnify the temperature field. Thermal radiative fluxing is employed wherein large temperature distinction is difference involved in getting enormous implementations in the medical field like thermal imaging, cryobiology, identification of breast tumors, peripheral vascular disorders, and diabetic neuropathy. It is quite interesting that when thermal radiation falls on the blood the temperature as well as heat transfer inside the blood escalates and dominates the viscosity phenomenon. Wastes excreted from cells get dissolved in the blood. The waste product occurs in the form of urea and creatinine. This type of waste material in the blood blockage the arteries. Thermal radiation falls on blood and enhances blood temperature removing these types of waste materials and opening the blocked arteries and blood is flowing easily through the arteries. Additional factors like the injection of hybridity nanomolecules in blood enhance the temperature of the fluid and heat deliverance and temperature field $\theta(\eta)$. Fig. 8S is designed to explore the effect of the Sisko fluid model parameter on $\theta(\eta)$. It is quite evident that magnification in S brings about a positive change in viscosity and thickens the blood. Viscosity is contrarywise associated with temperature. The temperature amplifies because of an increment change in S. Incremental temperature change provides additional heat to the blood which is utilized inside the blood to remove toxic material. Incremental change in the volume fraction of trihybrid nanoparticles also contributes in this sense. That's why a magnification in S amplifies the temperature field.

The impact of thermal relaxation variable λ_1 on temperature outline $\theta(\eta)$ is highlighted in Fig. 9S. It is observed that fluid becomes more viscous by the value of magnification in λ_1 and inclusion of nanomolecules in the standard liquid. Viscosity is inversely linked with temperature. A positive variation in λ_1 amplifies viscosity and diminishes the temperature of the fluid flow which brings about a reduction in temperature field $\theta(\eta)$. The effect of Rd and Ec on heat deliverance rate in the case of blood flow through arteries are highlighted in Figs. 7 and 8 separately. From Fig. 7 it is reflected that the heat transference increases in the case of magnification in Rd. More heat is produced inside the blood in the case of an increment changing in Rd which delivers more heat and increases the temperature of the fluid. More heat is delivered in the position of trihybridity nanoparticles contrary to dihybridity nanoparticles. Heat transfer diminishes in the case of the upswing in Ec. Frictional heat is produced when work is done by the blood against viscous stresses which amplifies temperature but diminishes the heat transfer rate and this decrement in heat transfer is much more obvious in the instance of dihybrid nanoparticles counter to dihybridity nanoparticles. Figs. 10S and 11S are designed to probe the outcomes of n and

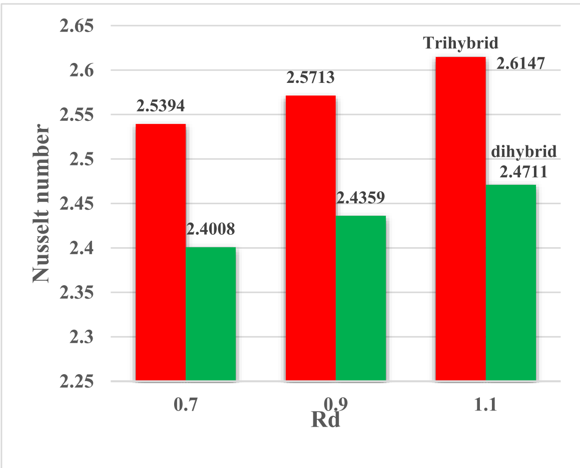

Fig. 7. Influence of Rd on heat transfer rate.

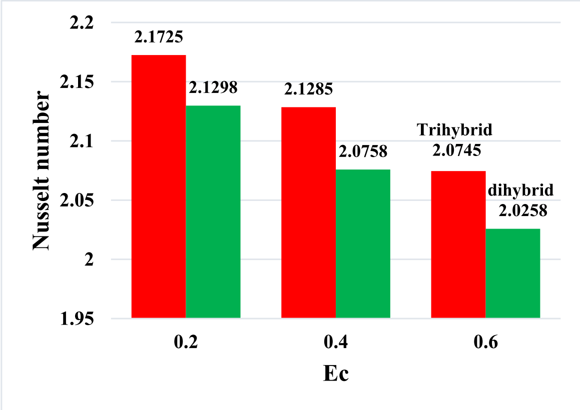

Fig. 8. Impact of Ec on heat transfer rate.

Table 2
Comparing analysis of obtained findings with Khan et al. [25] for the situation of surface drag factor.

γ	φ	$Cf_x Re_x^{\frac{-1}{2}}$ Present	Ref. [21]	$Relative\ error = \left\lvert \frac{Cf_x(pre) - Cf_x(ref)}{Cf_x(pre)} \right\rvert \times 100\%$
0.1	0.0	0.939500	0.939470	0.00325%
0.12		0.929573	0.929564	0.00009%
0.14		0.918049	0.918057	0.00007%
0.1	0.0	0.939468	0.939474	0.00006%
	0.05	1.323749	1.323756	0.00005%
	0.1	1.714000	1.714009	0.00004%

M on the drag friction phenomenon. The frictional occurrence is in reverse correlated to the velocity of blood flow through arteries. It is well recognized that elaboration in n and M strengthens the viscid of fluid that squeezes the arteries and produced a negative impact on the blood flow through arterial walls. The wall frictional factor depreciates in the situation of amplification in n and M respectively.

Table 2 is designed to reflect the comparative analysis of obtained results with Khan et al. [25] by keeping parameters like $S = M = \gamma = n = 0$. From comparison analysis, it is noted that the proposed scheme as well as the achieved outcomes are extremely acceptable and trustworthy. Relative error has been computed by taking a difference between numerically computed values and referenced values obtained from the literature over numerically computed values into hundred percent. From the relative error, it is observed that the obtained outcomes are quite authentic and reliable in contrast to the existing literature [25]. Table 3 reflects the performance of dihybrid and trihybrid nanoparticles in the case of heat transfer rate. In this table, it is seen that heat delivers considerably improved in the position of trihybridity nanoparticles in assessments a comparison with dihybridity nanoparticles. That's why the injection of trihybrid nanoparticles in the blood flow through arteries delivers more temperature and heat in contrast to dihybrid nanoparticles. Table 4 is constructed to reflect the influence of varied variables in the case of friction sensation and heat transport rate. The skin friction fact increases with the magnification in S, γ, Pr, Rd, Ec, λ_1 but diminishes in the case of n and M. The rate of heat transference amplifies in the case of Rd, Pr, n, M, λ_1 but diminishes in the case of γ and S.

6. Conclusion

The numerical details of the steadiness of laminar flowing and heat transmission attribute via boundary-layer of a one-phase Sisko ternary hybrid nanofluid (THNF) model (blood include Au, Ag, and TiO_2 NPs) with exponentially stretchable sheet has been described. The quantitative evaluations for all physical flow characteristics in terms of shear-thinning and shear-thickening were thoroughly presented. Computational observations have indicated that.

- Because of the amplification in S, the viscosity of blood progressively reduces, which has a positive effect on The human circulatory system and aids to avoid heart assaults and fast blows.
- The rapidity outline was reduced as the magnetic variable was boosted.
- A magnification in γ leads to an improvement in blood flowing rapidity, and blood flows more frequently through arteries, lowering the risk of heart attack and stroke.
- The temperature profile improved as the curvature parameter and the Eckert number increased.
- Propagation in Rd and trihybrid nanoparticles raises the average kinetic energy of the molecules, resulting in temperature field magnification.

Table 3
Testing of heat transport in the instance of tri- and di-hybrid nanostructures.

φ	Di-hybridity	$\varphi = \varphi_1 + \varphi_2 + \varphi_3$	Tri-hybridity
0.005	3.8015	0.1	4.2012
0.01	3.9897	0.11	4.3215
0.02	4.0122	0.12	4.4759
0.03	4.1867	0.13	4.6012

Table 4
Influence of diverse variables on frictional factor and heat transition sensation in tri-hybridity type.

S	M	γ	n	Pr	Rd	Ec	λ_1	$Cf_x Re_x^{\frac{1}{2}}$	$Nu_x Re_x^{\frac{-1}{2}}$
0.1	0.1	1	0.1	7	0.5	1.5	0.1	1.8756	3.9756
0.2								1.7564	3.8149
0.3								1.6451	3.5206
	0.3							1.7341	3.5730
	0.5							1.8259	3.6115
	0.7							1.9440	3.8596
		1.2						1.9123	3.8790
		1.4						2.1579	3.6142
		1.6						2.4263	3.4159
			0.3					1.8213	3.4159
			0.5					1.6015	3.6754
			0.7					1.4899	3.8855
				8				1.8579	3.9701
				9				1.9532	4.1254
				10				2.0157	4.3756
					1			1.8123	3.2156
					1.5			1.7259	3.4019
					2			1.7023	3.5213
						1.7		1.7802	3.7644
						1.9		1.8190	3.9190
						2.1		1.8301	4.1576
							0.5	1.8015	3.8765
							1.0	1.8576	3.9175
							1.5	1.9123	4.1213

- When Rd values increased significantly, the rate of heat transfer increased. However, when the physical parameters Ec were increased, the heat transfer rate decreased. In comparison to dihybrid nanoparticles, trihybrid nanoparticles deliver more heat.
- When n and M are increased, the surface drag phenomena decrease.
- Viscosity of fluid amplifies by the integrity of an increment in the thermal relaxation factor λ_1 which diminishes the temperature field.

In light of the present study, we develop the efforts to examine and explore the tetrahybrid nanofluid models to explore heat transference rate in the case of body liquid flowing via stenotic vessels as future works. Tumor detection, drug delivery, solar panels on the offshore oil rig. The model present in the current study has been employed to investigate the heat transfer rate of the fluid flow over various geometries like the fluid flow between two parallel disks, spinning spheres, wedges, and concentric cylinders. In the future, the existing method might be used to a number of physical and technical obstacles Refs. [56–64].

Author contributions

TS, WJ, and MRE formulated the problem. WJ and MRE solved the problem. FF, TS, WJ, MRE, GCA, IA, AAE and SMED calculated and inspected the outcomes. All the authors equally contributed to the writing and proofreading of the paper.

Availability of data

The manuscript has no associated data.

Declaration of competing interest

The authors declare that they have no known competing financial interests or personal relationships that could have appeared to influence the work reported in this paper.

Data availability

Data will be made available on request.

Acknowledgments

The authors extend their appreciation to the Deanship of Scientific Research at King Khalid University for funding this work through large group Research Project under grant number RGP2/251/44.

Nomenclature

Re	Reynolds number
T_w	wall temperature (K)
λ_1	Porosity parameter
Ec	Eckert number
Nu_x	Nusselt number
Pr	Prandtl number
Fr	Darcy-Forchheimer parameter
λ	buoyancy ratio parameter (N)
ρ_{hnf}	hybridity nanoliquid consistency $\left(\frac{kg}{m^3}\right)$
C_p	specific heat $(\frac{J}{kg.K})$
σ^*	Stefan-Boltzman constant $(\frac{W}{m^2K^4})$
M	Magnetic number
T_∞	free temperature (K)
β_1	fluid variable $(Pa.s)$
Gr	Grashof quantity
Cf_x	frictional force
Rd	radiative variable $(\frac{W}{m^3})$
q_r	radiation heating flux $(\frac{W}{m^2})$
γ	rapidity slippage $(\frac{m}{s})$
α_{hnf}	hybridity nanoliquid thermal diffusivity $(\frac{m^2}{s})$
k_{hnf}	thermal conductivity $(\frac{W}{m.K})$
κ^*	absorption coefficient $(\frac{1}{m})$

Appendix A. Supplementary data

Supplementary data to this article can be found online at https://doi.org/10.1016/j.csite.2023.103064.

References

[1] A. Abbasi, W. Farooq, E.M. Tag-El Din, S.U. Khan, M.I. Khan, K. Guedri, S. Elattar, M. Waqas, A.M. Galal, Heat transport exploration for hybrid nanoparticle (Cu, Fe_3O_4)—based blood flow via tapered complex wavy curved channel with slip features, Micromachines (9) (2022) 1415.

[2] L. Sarwar, A. Hussain, U. Fernandez-Gamiz, S. Akbar, A. Rehman, E.-S.M. Sherif, Thermal enhancement and numerical solution of blood nanofluid flow through stenotic artery, Sci. Rep. 12 (1) (2022), 17419.

[3] R. Padma, R.T. Selvi, R. Ponalagusamy, Effects of slip and magnetic field on the pulsatile flow of a Jeffrey fluid with magnetic nanoparticles in a stenosed artery, Eur. Phys. J. Plus 134 (5) (2019) 221.

[4] A. Saeed, A. Alsubie, P. Kumam, S. Nasir, T. Gul, W. Kumam, Blood based hybrid nanofluid flow together with electromagnetic field and couple stresses, Sci. Rep. (1) (2021) 1–18.

[5] I. Ullah, A. Ullah, M.M. Selim, M.I. Khan, Saima, A.A. Khan, M.Y. Malik, Analytical investigation of magnetized 2D hybrid nanofluid (GO+ ZnO+ blood) flow through a perforated capillary, Comput. Methods Biomech. Biomed. Eng. 25 (13) (2022) 1531–1543.

[6] P. Jalili, A. Sadeghi Ghahare, B. Jalili, D. Domiri Ganji, Analytical and numerical investigation of thermal distribution for hybrid nanofluid through an oblique artery with mild stenosis, SN Appl. Sci. 5 (4) (2023) 95.

[7] S. Ijaz, S. Nadeem, Biomedical theoretical investigation of blood mediated nanoparticles (Ag-Al2O3/blood) impact on hemodynamics of overlapped stenotic artery, Journal of Molecular Liquids248 (2017) 809–821.

[8] S.I. Abdelsalam, KhS. Mekheimer, A.Z. Zaher, Alterations in blood stream by electroosmotic forces of hybrid nanofluid through diseased artery: aneurysmal/stenosed segment, Chin, J. Phys. 67 (2020) 314–329.

[9] R. Gandhi, B.K. Sharma, C. Kumawat, O.A. Bég, Modeling and analysis of magnetic hybrid nanoparticle (Au-Al_2O_3/blood) based drug delivery through a bell-shaped occluded artery with joule heating, viscous dissipation and variable viscosity effects, P. I. Mech. Eng. E-J. Pro. 236 (5) (2022) 2024–2043.

[10] B.K. Sharma, R. Gandhi, T. Abbas, et al., Magnetohydrodynamics hemodynamics hybrid nanofluid flow through inclined stenotic artery, Appl. Math. Mech.-Engl. Ed. 44 (2023) 459–476.

[11] I. Shahzadi, S. Bilal, A significant role of permeability on blood flow for hybrid nanofluid through bifurcated stenosed artery: drug delivery application, Comput. Methods Progr. Biomed. 187 (2020), 105248.

[12] Soumini Dolui, Bivas Bhaumik, Soumen De, Combined effect of induced magnetic field and thermal radiation on ternary hybrid nanofluid flow through an inclined catheterized artery with multiple stenosis, Chem. Phys. Lett. 811 (2023), 140209.
[13] N. Saleem, T. Ashraf, I. Daqqa, S. Munawar, N. Idrees, F. Afzal, D. Afzal, Thermal case study of cilia actuated transport of radiated blood-based ternary nanofluid under the action of tilted magnetic field, Coatings (6) (2022) 873.
[14] S. Abeer, Alnahdi and Saleem Nasir and Taza Gul, Blood-based ternary hybrid nanofluid flow-through perforated capillary for the applications of drug delivery, Waves Random Complex Media (2022) 1–19.
[15] T. Sajid, W. Jamshed, M.R. Eid, G.C. Altamirano, F. Aslam, A.M. Alanzi, A. Abd-Elmonem, Magnetized Cross tetra hybrid nanofluid passed a stenosed artery with nonuniform heat source (sink) and thermal radiation: novel tetra hybrid Tiwari and Das nanofluid model, J. Magn. Magn Mater. 569 (2023), 170443.
[16] A. Riaz, S. Almutairi, S.E. Alhazmi, A. Saleem, S. Nadeem, A. Abdelrahman, Insight into the cilia motion of electrically conducting Cu-blood nanofluid through a uniform curved channel when entropy generation is significant, Alex. Eng. J. 61 (12) (2022) 10613–10630.
[17] N. Rathore, N. Sandeep, Computational framework on heat diffusion in blood-based hybrid nanoliquid flow through a stenosed artery: an aligned magnetic field application, Numer. Heat Transf. B: Fundam. 83 (2023) 162–175.
[18] A. Abidi, A. Ahmadi, M. Enayati, S.M. Sajadi, H. Yarmand, A. Ahmed, G. Cheraghian, A review of the methods of modeling multi-phase flows within different microchannels shapes and their applications, Micromachines (9) (2021) 1113.
[19] R. Gandhi, B.K. Sharma, N.K. Mishra, Q.M. Al-Mdallal, Computer simulations of EMHD Casson nanofluid flow of blood through an irregular stenotic permeable artery: application of koo-kleinstreuer-Li correlations, Nanomaterials 13 (2023) 652.
[20] A.W. Sisko, The flow of lubricating greases, Ind. Eng. Chem. (12) (1958) 1789–1792.
[21] L. Sarwar, A. Hussain, Flow characteristics of Au-blood nanofluid in stenotic artery, Int. Commun. Heat Mass Tran. 127 (2021), 105486, 2021.
[22] Abdulmajeed Almaneea, Numerical study on thermal performance of Sisko fluid with hybrid nano-structures, Case Stud. Therm. Eng. 30 (2022), 101754.
[23] L.K. Foong, N. Shirani, D. Toghraie, M. Zarringhalam, M. Afrand, Numerical simulation of blood flow inside an artery under applying constant heat flux using Newtonian and non-Newtonian approaches for biomedical engineering, Comput. Methods Progr. Biomed. 190 (2020), 105375.
[24] H. Waqas, U. Farooq, T. Muhammad, U. Manzoor, Importance of shape factor in Sisko nanofluid flow considering gold nanoparticles, Alex. Eng. J. 61 (2022) 3665–3672.
[25] M. Bilal, A. Saeed, Numerical computation for the dual solution of Sisko hybrid nanofluid flow through a heated shrinking/stretching porous disk, Int. J. Ambient Energy 43 (1) (2022) 8802–8811.
[26] A.F. Elelamy, N.S. Elgazery, R. Ellahi, Blood flow of MHD non-Newtonian nanofluid with heat transfer and slip effects: application of bacterial growth in heart valve, Int. J. Numer. Methods Heat Fluid Flow (11) (2020) 4883–4908.
[27] S.M. Abo-Dahab, R.A. Mohamed, A.M. Abd-Alla, et al., Double-diffusive peristaltic MHD Sisko nanofluid flow through a porous medium in presence of non-linear thermal radiation, heat generation/absorption, and Joule heating, Sci. Rep. 13 (2023) 1432.
[28] D. Kumar, B. Satyanarayana, R. Kumar, S. Kumar, N. Deo, Application of Heat source and chemical reaction in MHD blood flow through permeable bifurcated arteries with inclined magnetic field in tumor treatments, Results Appl. Math. 10 (2021), 100151.
[29] Y. Dadhich, R. Jain, S. Gyeltshen, Insights of heat and mass transfer in magneto-mixed convective Sisko nanofluid over a wedge with viscous dissipation, Math. Probl Eng. 2022 (2022) 13.
[30] S. Majeed, F. Ali, A. Imtiaz, I. Khan, M. Andualem, Fractional model of MHD blood flow in a cylindrical tube containing magnetic particles, Sci. Rep. 12 (1) (2022) 418.
[31] A. Tanveer, M. Khan, T. Salahuddin, M.Y. Malik, F. Khan, Theoretical investigation of peristaltic activity in MHD based blood flow of non-Newtonian material, Comput. Methods Progr. Biomed. 187 (2020), 105225.
[32] Junfeng Yin, M. Xianqin Zhang, Israr Ur Rehman, Aamir Hamid, Thermal radiation aspect of bioconvection flow of magnetized Sisko nanofluid along a stretching cylinder with swimming microorganisms, Case Stud. Therm. Eng. 30 (2022), 101771.
[33] Latif Ahmad, Masood Khan, Importance of activation energy in development of chemical covalent bonding in flow of Sisko magneto-nanofluids over a porous moving curved surface, Int. J. Hydrogen Energy 44 (2019) 10197–10206.
[34] C. Kumawat, B.K. Sharma, Q.M. Al-Mdallal, M. Rahimi-Gorji, Entropy generation for MHD two phase blood flow through a curved permeable artery having variable viscosity with heat and mass transfer, Int. Commun. Heat Mass Tran. 133 (2022), 105954.
[35] P. Sreedevi, P. Sudarsana Reddy, A.J. Chamkha, Heat and mass transfer analysis of nanofluid over linear and non-linear stretching surfaces with thermal radiation and chemical reaction, Powder Technol. 315 (2017) 194–204.
[36] S.K. Asha, G. Sunitha, Influence of thermal radiation on peristaltic blood flow of a Jeffrey fluid with double diffusion in the presence of gold nanoparticles, Inform. Med. Unlocked 17 (2019), 100272.
[37] A.M. Abd-Alla, S.M. Abo-Dahab, Esraa N. Thabet, M.A. Abdelhafez, Impact of Inclined Magnetic Field on Peristaltic Flow of Blood Fluid in an Inclined Asymmetric Channel in the Presence of Heat and Mass Transfer, Waves Random Complex Media, 2022, https://doi.org/10.1080/17455030.2022.2084653.
[38] Devendra Kumar, B. Satyanarayana, Rajesh Kumar, Sanjeev Kumar, Narendra Deo, Application of heat source and chemical reaction in MHD blood flow through permeable bifurcated arteries with inclined magnetic field in tumor treatments, Results Appl. Math. 10 (2021), 100151.
[39] N. Saleem, T. Ashraf, I. Daqqa, S. Munawar, N. Idrees, F. Afzal, D. Afzal, Thermal case study of cilia actuated transport of radiated blood-based ternary nanofluid under the action of tilted magnetic field, Coatings 12 (2022) 873.
[40] S. Manjunatha, V. Puneeth, , Ammani Kuttan Baby, C.S. Vishalakshi, Examination of Thermal and Velocity Slip Effects on the Flow of Blood Suspended with Aluminum Alloys over a Bi-directional Stretching Sheet: the Ternary Nanofluid Model, Waves Random Complex Media, 2022, https://doi.org/10.1080/17455030.2022.2056260.
[41] R. Gandhi, B.K. Sharma, C. Kumawat, O.A. Bég, Modeling and analysis of magnetic hybrid nanoparticle (Au-Al_2O_3/blood) based drug delivery through a bell-shaped occluded artery with joule heating, viscous dissipation and variable viscosity effects, P. I. Mech. Eng. E-J. Proc. (2022), 09544089221080273.
[42] N.A. Zainal, R. Nazar, K. Naganthran, I. Pop, Magnetic impact on the unsteady separated stagnation-point flow of hybrid nanofluid with viscous dissipation and joule heating, Mathematics 10 (2022) 2356.
[43] G. Venkatesan, A.S. Reddy, Insight into the dynamics of blood conveying alumina nanoparticles subject to Lorentz force, viscous dissipation, thermal radiation, Joule heating, and heat source, Eur. Phys. J. Spec. Top. 230 (5) (2021) 1475–1485.
[44] I. Waini, U. Khan, A. Zaib, A. Ishak, I. Pop, Thermophoresis particle deposition of CoFe2O4-TiO2 hybrid nanoparticles on micropolar flow through a moving flat plate with viscous dissipation effects, Int. J. Numer. Methods Heat Fluid Flow 32 (2022) 3259–3282.
[45] V. Sridhar, K. Ramesh, D. Tripathi, V. Vivekanand, Analysis of thermal radiation, Joule heating, and viscous dissipation effects on blood-gold couple stress nanofluid flow driven by electroosmosis, Heat Transf 51 (5) (2022) 4080–4101.
[46] C. Sulochana, Geeta C. Shivapuji, Numerical analysis of hybrid nanofluid flow over a nonlinear stretching sheet with viscous dissipation, joule heating effects, CFD Lett. 14 (10) (2022) 43–55, 2022.
[47] M.I. Anwar, K. Rafique, M. Misiran, et al., Keller-box analysis of inclination flow of magnetized Williamson nanofluid, SN Appl. Sci. 2 (2020) 377.
[48] M. Arif, A. Saeed, P. Suttiarporn, et al., Analysis of second grade hybrid nanofluid flow over a stretching flat plate in the presence of activation energy, Sci. Rep. 12 (2022), 21565.
[49] Q.H. Shi, T. Shabbir, M. Mushtaq, et al., Modelling and numerical computation for flow of micropolar fluid towards an exponential curved surface: a Keller box method, Sci. Rep. 11 (2021), 16351, https://doi.org/10.1038/s41598-021-95859-x.
[50] W. Jamshed, M.R. Eid, K.S. Nisar, N.A.A.M. Nasir, A. Edacherian, C.A. Saleel, V. Vijayakumar, A numerical frame work of magnetically driven Powell-Eyring nanofluid using single phase model, Scientific reports11 (1) (2021) 1–26.
[51] B. Ahmed, F. Akbar, A. Ghaffari, Sami Ullah Khan, M. Ijaz Khan, Y. Dharmendar Reddy, Soret and Dufour Aspects of the Third-Grade Fluid Due to the Stretching Cylinder with the Keller Box Approach, Waves in Random and Complex Media, 2022, https://doi.org/10.1080/17455030.2022.2085891.
[52] F.A. Alwawi, M.Z. Swalmeh, A.S. Qazaq, R. Idris, Heat transmission reinforcers induced by MHD hybrid nanoparticles for water/water-EG flowing over a cylinder, Coatings (6) (2021) 623.

[53] I. Ullah, I. Khan, S. Shafie, Heat and mass transfer in unsteady MHD slip flow of Casson fluid over a moving wedge embedded in a porous medium in the presence of chemical reaction: numerical Solutions using Keller-Box Method, Numer. Methods Part. Differ. Equ. 34 (2018) 1867–1891.
[54] T. Shabbir, M. Mushtaq, M. Ijaz Khan, T. Hayat, Modeling and numerical simulation of micropolar fluid over a curved surface: Keller box method, Comput. Methods Progr. Biomed. (2020 Apr) 187 105220, https://doi.org/10.1016/j.cmpb.2019.105220.PMID:31790945.
[55] G. Kumaran, R. Sivaraj, V.R. Prasad, O.A. Beg, H.-H. Leung, F. Kamalov, Numerical study of axisymmetric magneto-gyrotactic bioconvection in non-Fourier tangent hyperbolic nano-functional reactive coating flow of a cylindrical body in porous media, The European Physical Journal Plus136 (11) (2021) 1107.
[56] A. Aziz, W. Jamshed, T. Aziz, H.M.S. Bahaidarah, K.U. Rehman, Entropy analysis of powell-eyring hybrid nanofluid including effect of linear thermal radiation and viscous dissipation, J. Therm. Anal. Calorimetry 143 (2020) 1331–1343.
[57] W. Jamshed, S. U, S. Devi, M. Goodarzi, M. Prakash, K.S. Nisar, M. Zakarya, A.H. Abdel-Aty, Evaluating the unsteady Casson nanofluid over a stretching sheet with solar thermal radiation: an optimal case study, Case Stud. Therm. Eng. 26 (2021), 101160.
[58] W. Jamshed, K. S, R. Nisar, J.P. Gowda, R.N. Kumar, B.C. Prasannakumara, Radiative heat transfer of second grade nanofluid flow past a porous flat surface: a single-phase mathematical model, Phys. Scripta 96 (2021), 064006.
[59] W. Jamshed, K.S. Nisar, R.W. Ibrahim, T. Mukhtar, V. Vijayakumar, F. Ahmad, Computational frame work of Cattaneo-Christov heat flux effects on Engine Oil based Williamson hybrid nanofluids: a thermal case study, Case Stud. Therm. Eng. 26 (2021), 101179.
[60] W. Jamshed, S.U. Devi, K.S. Nisar, Single phase-based study of Ag-Cu/EO Williamson hybrid nanofluid flow over a stretching surface with shape factor, Phys. Scripta 96 (2021), 065202.
[61] S.M. Hussain, W. Jamshed, A comparative entropy-based analysis of tangent hyperbolic hybrid nanofluid flow: implementing finite difference method, Int. Commun. Heat Mass Tran. 129 (2021), 105671.
[62] F.Z. Wang, M.I. Asjad, M. Zahid, A. Iqbal, H. Ahmad, M.D. Alsulami, Unsteady thermal transport flow of Casson nanofluids with generalized Mittag-Leffler kernel of Prabhakar's type, J. Mater. Res. Technol. 14 (2021) 1292–1300.
[63] F.Z. Wang, E.R. Hou, S.A. Salama, M.M.A. Khater, Numerical investigation of the nonlinear fractional ostrovsky equation, Fractals 30 (5) (2022), 22401429.
[64] F.Z. Wang, A.M. Saeed, V. Puneeth, N.A. Shah, M.S. Anwar, K. Geudri, S.M. Eldin, Heat and mass transfer of Ag−H2O nano-thin film flowing over a porous medium: a modified Buongiorno's model, Chin. J. Phys. (2023), https://doi.org/10.1016/j.cjph.2023.01.001.